This is the accepted manuscript made available via CHORUS. The article has been published as:

Cluster Synchronization in Multilayer Networks: A Fully Analog Experiment with LC Oscillators with Physically Dissimilar Coupling

Karen A. Blaha, Ke Huang, Fabio Della Rossa, Louis Pecora, Mani Hossein-Zadeh, and Francesco Sorrentino

Phys. Rev. Lett. **122**, 014101 — Published 4 January 2019

DOI: 10.1103/PhysRevLett.122.014101

Cluster Synchronization in Multilayer Networks: A fully analog experiment with LC Oscillators with Physically Dissimilar Coupling

Karen A. Blaha[1], Ke Huang[2], Fabio Della Rossa[1,3], Louis Pecora[4], Mani Hossein-Zadeh[2], and Francesco Sorrentino[1,2]
[1]*Department of Mechanical Engineering, University of New Mexico, Albuquerque, New Mexico 87131, USA*
[2]*Department of Electrical and Computer Engineering, University of New Mexico, Albuquerque, New Mexico 87131, USA*
[3]*Politecnico di Milano, Piazza Leonardo da Vinci 32, Milano, Italy*
[4]*U.S. Naval Research Laboratory, Washington, DC 20375, USA*
(Dated: November 20, 2018)

We investigate cluster synchronization in experiments with a multilayer network of electronic Colpitts oscillators, specifically a network with two interaction layers. We observe and analytically characterize the appearance of several cluster states as we change coupling in the layers. In this study, we innovatively combine bifurcation analysis and the computation of transverse Lyapunov exponents. We observe four kinds of synchronized states, from fully synchronous to a clustered quasiperiodic state—the first experimental observation of the latter state. Our work is the first to study fundamentally dissimilar kinds of coupling within an experimental multilayer network.

PACS numbers: May be entered using the \pacs{#1} command.

Networks with multiple layers of interactions arise in models for epidemic propagation [1, 2], the social world of the Medicis [3], and the failure of interdependent networks such as the power grid [4, 5], among others. These layers of interactions can operate in fundamentally different ways. Neurons communicate by both chemical and electrical coupling; chemical synapses are probabilistic, delayed, and unidirectional while electrical synapses are deterministic and bidirectional [6]. The interplay between both kinds of synapses is thought to be essential to normal functioning of the brain [6–8].

Networks with a high number of symmetries arise in many systems [9]: in biology, the *C. elegans* metabolic network; in infrastructure the U.S. power grid and airport network; in social networks, the PhD network [10]. Symmetric multilayer networks have been investigated using quotient networks for dimensionality reduction [11, 12] and using eigenspectral analysis [11]. Study of synchronization in multilayer networks was originally presented in [13, 14] and more recently in [15]. Recent experiments explored synchronization between identical [16] and non-identical [17] layers of a multilayer network. These papers studied complete synchronization (all systems synchronizing on the same time-evolution) with only diffusive coupling.

Clustered patterns arise from network symmetries [18, 19], but few experiments study this causality; most experimental studies focus solely the appearance of interesting clusters and not on the role the network symmetries play in their presence [20–22]. The studies that do directly connect network symmetry and clustering are digitally implemented [18, 23, 24]; they exclude some aspects that arise in real systems. No experimental study of clustering in multilayer networks exists.

In this letter, we are the first to study cluster synchronization in a fully analog symmetrical multilayer network with both diffusive and non-diffusive coupling. Despite of its simplicity, this analog electronic system not only represents the smallest multilayer network with multiple symmetries but also captures the uncertainties and fluctuations present in real and more complex physical systems. We describe the possible cluster synchronizations of the system as we vary coupling parameters. We experimentally observe and theoretically characterize clusters of nodes that synchronize on different time evolutions. The system is fully analog, where other studies have used a computer interface to implement coupling [16, 17, 25].

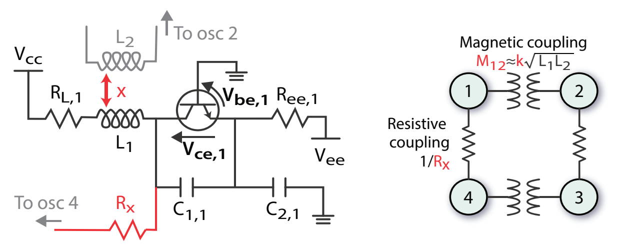

FIG. 1. Left panel: Colpitts oscillator. The oscillator is coupled to its two neighbors via resistor R_x and mutual magnetic coupling between the tank inductors, controlled by the inductor separation, x. Tunable parameters are in red; fixed components of other oscillators are in gray. Right panel: Topology of the coupled oscillator network. $M_{ij} = k\sqrt{L_i L_j}$, where k is roughly proportional to $1/x^2$.

Electronic circuits are ideal testbeds for the study of nonlinear behavior in networks [26]; we choose to use the Colpitts oscillator. As shown in the left panel of Fig. 1, the Colpitts oscillator is a simple electronic oscillator based on a bipolar junction transistor (BJT) that uses two center-tapped capacitors in series with a parallel inductor as its resonance tank circuit. Several studies have explored the periodic, quasi-periodic and chaotic behavior of individual Colpitts oscillators [27–30]. Others have discussed either magnetically coupled [31] or resistively coupled [30] Colpitts oscillators. Simplicity, low-cost, ease of fabrication, ability to work in different regimes, availability of a large volume of previous studies, and the ability to introduce different kinds of connections make the Colpitts oscillator particularly suitable for multilayer network studies. We create the first fully-analog multilayer network with four periodic Colpitts oscillators coupled through two different kinds of coupling mechanisms, resistive and magnetic.

The right panel of Fig. 1 shows the topology of the corresponding network; this is the simplest multilayer network that has multiple symmetries (for an easier network with only one symmetry, see SI Sec. 2). The four nodes, each a Colpitts oscillator, form a ring with coupling alternating between resistive and magnetic. We achieve resistive coupling by connecting the collectors of transistors in pairs of oscillators through a resistor, R_x; we tune the coupling by connecting resistors of the desired value. To achieve magnetic coupling, we bring the inductors of two nodes sufficiently near, such that the mutual inductance, M_{ij}, becomes large enough; we tune the coupling by changing the inductor separation distance, x.

The dynamics of the network shown in Fig. 1 is:

$$\begin{aligned}
C_{1,i}\dot{V}_{ce,i} &= I_{L,i} - I_c(V_{be,i}) \\
&\quad + \frac{1}{R_x}\sum_{j=1}^{N}\mathbb{R}_{ij}[(V_{ce,j}-V_{ce,i})-(V_{be,j}-V_{be,i})] \\
C_{2,i}\dot{V}_{be,i} &= -(V_{ee}+V_{be,i})/R_{ee,i} - I_b(V_{be,i}) - I_{L,i} \qquad (1)\\
&\quad - \frac{1}{R_x}\sum_{j=1}^{N}\mathbb{R}_{ij}[(V_{ce,j}-V_{ce,i})-(V_{be,j}-V_{be,i})] \\
L_i\dot{I}_{L,i} &= V_{cc} - V_{ce,i} + V_{be,i} - I_{L,i}R_{L,i} - \sum_{j=1}^{N}M_{ij}\mathbb{M}_{ij}\dot{I}_{L,j},
\end{aligned}$$

where $i = 1, ..., 4$ is the index of the oscillator, L_i is the inductance and $C_{1,i}$, $C_{2,i}$ are the capacitances of the circuit components (see Fig. 1); $V_{ce,i}$ is the voltage drop between the collector and the emitter of the transistor; $V_{be,i}$ is the voltage drop between the base and the emitter. V_{cc} and V_{ee} are applied voltages; I_b and I_c are the current of the base and the collector, respectively. These two currents are the nonlinear terms in the system; they are zero below a threshold voltage and increase linearly above this cutoff. In a BJT these currents are related through $\beta = \Delta I_c/\Delta I_b \approx I_c/I_b$ where β is the BJT amplification factor, see SI for more details about the experimental arrangement.

The magnitudes of the resistive and magnetic coupling coefficients are $1/R_x$ and $M_{ij} = k\sqrt{L_iL_j}$, respectively. k characterizes the mutual inductance and is roughly proportional to $1/x^2$ (see SI for a specific relationship); k is positive if the currents induced by mutual and self-inductance are in-phase, and negative if they are antiphase. Note that the resistive and magnetic couplings are different in nature and therefore enter the dynamic equations in different forms (as evident in Eq. (1)). Resistive coupling is diffusive and affects the current. Magnetic coupling is non-diffusive, differential [32], and affects the voltage. The adjacency matrices $\mathbb{R}$ and $\mathbb{M}$ describe how the oscillators are connected to one another by resistive and magnetic coupling, respectively. In our four-member ring network, $\mathbb{R}$ and $\mathbb{M}$ are:

$$\mathbb{R} = \begin{bmatrix} 0&0&0&1\\ 0&0&1&0\\ 0&1&0&0\\ 1&0&0&0 \end{bmatrix}, \quad \mathbb{M} = \begin{bmatrix} 0&1&0&0\\ 1&0&0&0\\ 0&0&0&1\\ 0&0&1&0 \end{bmatrix}. \qquad (2)$$

By inspection of the four-node system (right panel of Fig. 1), we observe three symmetries present in the multilayer network, *i.e.,* three permutations of the nodes which leave the network unchanged: (1) vertical symmetry, permuting 1 with 4 and 2 with 3, (2) 180° rotation, permuting 1 with 3 and 2 with 4, (3) horizontal symmetry, permuting 1 with 2 and 3 with 4. These permutations, along with the identical permutation (that maps each node to itself), form a mathematical group $\mathcal{G}$ that we call *symmetry group of the multilayer network*. Subgroups of $\mathcal{G}$ define possible cluster patterns [25].

By assuming the Colpitts oscillators have identical components ($C_{1,i} = C_{2,i} = C$, $L_i = L$, $M_{ij} = M_{ji} = M = kL$), we can rewrite Eq. (1) as a generic multidimensional network with $N = 4$ oscillators coupled through $\Lambda = 2$ layers [13–15, 33, 34] (see SI for derivation):

$$\dot{\boldsymbol{x}}_i = F(\boldsymbol{x}_i) + \sum_{\lambda=1}^{\Lambda}\sigma^{(\lambda)}\sum_{j=1}^{N}A_{ij}^{(\lambda)}H^{(\lambda)}(\boldsymbol{x}_j), \qquad (3)$$

where

$$\boldsymbol{x}_i = \begin{bmatrix} V_{ce,i}\\ V_{be,i}\\ I_{L,i} \end{bmatrix}, \; F = \begin{bmatrix} \frac{-I_c(V_{be,i})+I_{L,i}}{C}\\ \frac{-(V_{ee}+V_{be,i})/R_{ee}-I_b(V_{be,i})-I_{L,i}}{C}\\ \frac{V_{cc}-V_{ce,i}+V_{be,i}-I_{L,i}R_L}{L(1-k^2)} \end{bmatrix},$$

$$H^{(1)} = \begin{bmatrix} V_{ce}-V_{be}\\ V_{be}-V_{ce}\\ 0 \end{bmatrix}, \; H^{(2)} = \begin{bmatrix} 0\\ 0\\ V_{cc}-V_{ce}+V_{be}-I_LR_L \end{bmatrix},$$

$\sigma^{(1)} = \frac{1}{CR_x}$, $\sigma^{(2)} = -\frac{k}{L(1-k^2)}$, $A^{(1)} = \mathbb{R} - I_4$ and $A^{(2)} = \mathbb{M}$, where I_4 is the 4 dimensional identity matrix.

Let the clustered motion have C clusters, $\mathcal{C}_1, \ldots, \mathcal{C}_C$, and let $\boldsymbol{s}(t) = s_1(t), s_2(t), \ldots, s_C(t)$ be a possible clustered solution. We can linearize Eq. (3) around that solution obtaining

$$\delta\dot{\boldsymbol{x}} = \Bigg[\sum_{n=1}^{C}E_n\otimes DF(s_n) + \sum_{\lambda=1}^{\Lambda}\sigma^{(\lambda)}\left(A^{(\lambda)}\otimes I_3\right)\sum_{n=1}^{C}\left(E_n\otimes DH^{(\lambda)}(s_n)\right)\Bigg]\delta\boldsymbol{x}, \qquad (4)$$

where E_n is a four by four matrix which identifies if node i belongs to cluster $\mathcal{C}_n$ ($E_n(i,i) = 1$ if $i \in \mathcal{C}_n$, 0 otherwise). D represents the Jacobian operator.

Using the coordinate change $\delta\boldsymbol{\eta} = (T \otimes I_3)\delta\boldsymbol{x}$, we convert Eq. (4) from the node coordinate system to the irreducible representation (IRR) coordinate system. The IRR simultaneously block-diagonalizes the permutation matrices in the symmetry group of the multilayer network $\mathcal{G}$; each block is an irreducible representation of the group [35]. Eq. (4) becomes

$$\delta\dot{\boldsymbol{\eta}} = \Bigg[\sum_{n=1}^{C} J_n \otimes DF(s_n) + \sum_{\lambda=1}^{\Lambda} \sigma^{(\lambda)} \left(B^{(\lambda)} \otimes I_3\right) \sum_{n=1}^{C} \left(J_n \otimes DH^{(\lambda)}(s_n)\right)\Bigg] \delta\boldsymbol{\eta}, \tag{5}$$

where $J_n = TE_nT^{-1}$ and $B^{(\lambda)} = TA^{(\lambda)}T^{-1}$. This change of coordinates decouples the dynamics of perturbations along the synchronous manifold from those transverse to it, allowing us to separately analyze each direction [25].

We perform the cluster synchronization analysis in two steps. First, we characterize global behavior along the synchronous manifold by studying the bifurcations of the nonlinear equations for each quotient network [36]. In the quotient network, all the nodes belonging to the same cluster (*i.e.,* synchronized) are represented by one node, since their dynamics and their coupling with other clusters of the network is identical. We compute all the possible solutions by starting simulations from many initial conditions, and we characterize the stability of each solution with a complete bifurcation analysis. We use AUTO07P[37, 38] to locate bifurcations and then MATCONT to compute their normal form coefficients [39–41].

Second, we analyze the transverse block of Eq. (5); we compute the Maximum Lyapunov Exponent [42] of the subsystem, evaluating Eq. (5) at each synchronous stable solution $\boldsymbol{s}_n$ for all the possible parameter pairs. We need the global analysis to characterize all the possible solutions along which we compute the variational equation (see SI for a detailed description of the analysis).

Figure 2 shows the four possible cluster patterns. For each pattern, the quotient network dynamics is described by Eq. (3) with a suitable choice of the coupling matrices $A^{(1)}$ and $A^{(2)}$. We also report the matrices, T, needed for the study of the stability transverse to each synchronous solution. To assess the stability of the clustered solutions, we analyze only the three possible two-cluster quotient networks. The fully synchronized pattern is a special solution of all three two-cluster quotient networks, and we can thus obtain its stability by looking at the stability of each of the other patterns.

In Figure 3, we show the combined analysis of the three clustered solutions, grouped into in-phase (left) and anti-phase (right) solutions (see the SI for a detailed analysis of the three clustered solutions, where we present and explain each bifurcation diagram and transverse stability diagram). We identify nine regions with qualitatively different clustered patterns (reported in the bottom boxes of Fig. 3). We group the cluster patterns to relate them

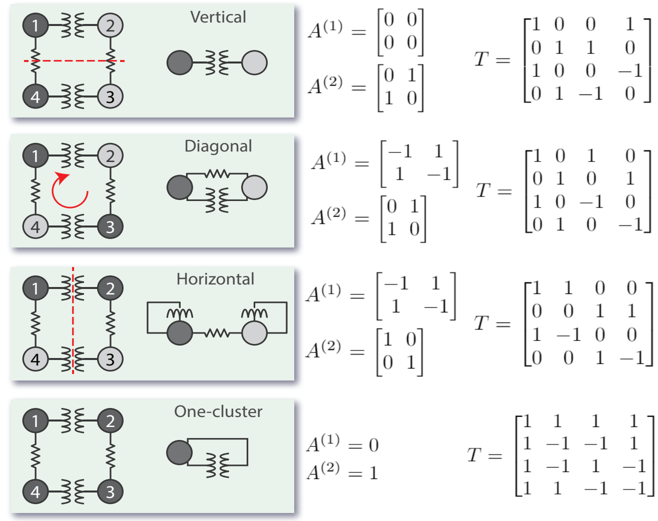

FIG. 2. Possible cluster synchronization patterns. The left schematic represents the full network; nodes belonging to the same cluster synchronization pattern are colored the same. We indicate symmetry with the red dashed line. The one- or two-node labeled schematic represents the quotient network. On the right, we show the $A^{(\lambda)}$ and T for each pattern. $A^{(\lambda)}$ is the adjacency matrix for layer λ, with $\lambda = 1$ representing the resistive layer and $\lambda = 2$ representing the magnetic layer.

to experimentally observable behavior; this is because some of the cluster states become indistinguishable in the presence of experimental noise and heterogeneity. For example, cluster patterns a_1 and a_2 differ by a small phase offset that cannot be measured due to experimental noise. Cluster patterns a_1 and a_3 differ mostly in amplitude, but the experimental amplitude is sensitive to many details beyond the scope of the model, such as the resistances of the capacitors, inductors, and component junctions, and nonlinearity of the transistor gain. We thus create four groups from the nine theoretical clustered patterns— (a, gray) fully in-phase, tolerating small mismatches in amplitude and phase; (b, turquoise) the vertical two-cluster with a phase offset up to $\pi/2$ rad; (c, pink) the vertical two-cluster, tolerating small mismatches in amplitude and phase; and (d, magenta) the quasiperiodic vertical two-cluster, tolerating small mismatches in amplitude.

We performed experiments at 5 values of R_x (27Ω, 300Ω, 510Ω, 750Ω, and 1000Ω) and varied k from -0.03 to -0.4 for the parallel inductor configuration and from 0.03 to 0.4 for the anti-parallel inductor configuration. To detect the presence of multiple attractors we first increase then decrease k, guided by the theoretically predicted hysteresis between the periodic in-phase and the periodic anti-phase solutions (in the left panel of Fig. 3 no in-phase solution is present for large negative k, while in the right panel no anti-phase solution is present for large positive k). The top left panel of Fig. 4 shows the cluster state observed at each experimental measurement.

Figure 4 shows broad agreement between our experi-

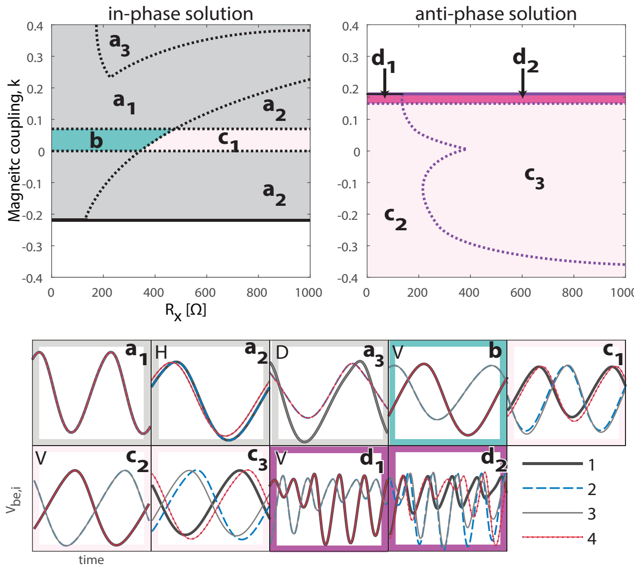

FIG. 3. Possible patterns of Eq. (3). Region coloring indicates experimentally distinguishable patterns: (Top left) in-phase and (Top right) antiphase. Boxes below show representative time series from simulations grouped by observability. When clustered solutions are present, we indicate them with V, H, or D in the upper lefthand corner for vertically-, horizontally-, and diagonally- synchronized, respectively. (a panels) gray: in-phase, tolerating small mismatches in amplitude and phase; (b panel) turquoise: vertical two-cluster with a phase offset up to $\pi/2$ rad; (c panels) pink: vertical two-cluster, tolerating small mismatches in amplitude and phase; (d panels) magenta: quasiperiodic vertical two-cluster, tolerating small mismatches in amplitude.

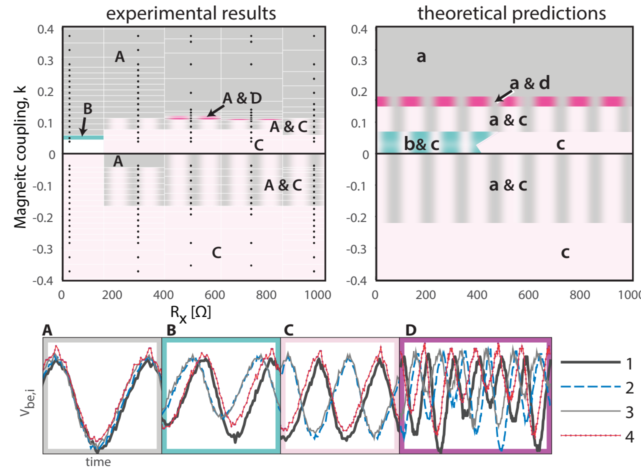

FIG. 4. Gray represents the one-cluster state; pink represents the vertical two-cluster state; turquoise represents a solution of the vertical two-cluster state two-cluster with a phase offset up to $\pi/2$; magenta represents a quasi-periodic solution of the vertical two-cluster state; and white represents no stable frequency locking. Stripes of two colors represent bistability between the two states represented by each color. (Top left) Experimentally observed cluster states. Black dots represent individual experimental measurements; we infer a color mesh from these results. (Top right) Theoretical prediction of cluster states from Fig. 3. (Bottom) Experimental time series of $V_{be}(t)$ demonstrating clusters corresponding to the theoretical predictions. From left to right, we observe (A) the fully synchronized state, (B) the vertical two-cluster with a phase offset up to $\pi/2$ rad, (C) the two-cluster, and the (D) quasi-periodic two-cluster.

mental and theoretical results (for discussion of the discrepancies, see the SI). Each of the four cluster types (reported in the bottom boxes of Fig. 4) observed experimentally is predicted by the theoretical analysis. The system exhibits bistability between the fully synchronized state (A, gray) and the vertical two-cluster state (C, pink) for large ranges of k and R_x. We observe the fully synchronized solution for large positive magnetic coupling and small negative coupling; we observe the vertical two-cluster solution for small positive and large negative coupling. Near $k = 0.12$, we see the quasiperiodic vertical two-cluster state (D, magenta). At $k = 0.05$ and $R_x = 27\Omega$, we observe the vertical two-cluster with a phase separation near $\pi/2$ rad, (B, turquoise).

This work is the first study on cluster synchronization in multilayer networks with symmetries. We show that a small network with well-understood periodic Colpitts oscillators exhibits rich dynamical behavior such as bistability, hysteresis, and quasiperiodicity. This is the first experimental observation of a clustered quasiperiodic state. The analysis innovatively combines bifurcation analysis and the computation of transverse Lyapunov exponents, allowing us to overcome limitations of each individual approach. First, unlike the bifurcation analysis of the full system, our approach can handle multiple symmetries using standard software [37, 39]. Second, compared to the computation of transverse Lyapunov exponents alone, it can find any possible cluster pattern even in the presence of multiple attractors of the quotient networks. The interplay of theory and experiments was essential for an in-depth phenomenological understanding of the system behavior; experiments allowed us to understand which theoretically predicted cluster states were observable, while theory helped us identify hard to find cluster states. Note that even though we have applied our analysis to a very simple multilayer network, it is possible to scale the described approach to networks with any numbers of nodes or layers. This scaling is nontrivial and requires the definition of the group of symmetries of a multilayer network; this is the subject of ongoing research and is briefly introduced in the SI, sect 5 [43].

Our work shows how different interactions layers influence the overall state of the system; applications of the described theory can be found in a variety of fields where patterned behavior and multilayer systems arise. The method requires three ingredients: (1) a dynamical system describing the network, (2) multiple kinds of interactions, and (3) patterned behavior. Many papers propose dynamical equations for both neurons [44–46] and their network of interactions [47–50]; neurons are connected through electrical and chemical synapses [6]. A vast literature explores the likely relationship between epilepsy and synchronization [51] and models of coupled neurons exhibit clustered behavior [52]. Several models exist to describe the dynamics of opinion formation [53, 54], which is mediated by different layers of interaction through social media, advertising, friend networks, *etc.*, producing clusters of belief [55]. Bark beetles infest forests in patterns [56]; different tree species and various beetle transportation methods (self, carried by animals or wind, *etc.*) form the multilayer network representation of the forest-insect model [57]. Proposed circuit designs use quantum cellular automata (QCA) with cluster-like clock zones to perform calculations; two kinds of QCA cells (regular and rotated) are connected with either coplanar or multilayer connections [58]. Understanding the dynamical behavior of symmetric multilayer networks may play an important role in the design and development of neuromorphic computational systems [59]. To our knowledge, none of the studies on neuromorphic systems has considered dissimilar interactions between nodes, which seems to be an essential feature of most biological networks such as the brain [6] as well as a contributor to the overall robustness of a system [60, 61].

ACKNOWLEDGMENTS

This work was supported by the National Science Foundation (award number 1727948).

[1] F. Ball and P. Neal, Math. Biosci. **212**, 69 (2008).

[2] W. Wang, M. Tang, H. Yang, Y. Do, Y.-C. Lai, and G. Lee, Sci. Rep. **4**, 5097 (2014).

[3] J. F. Padgett and C. K. Ansell, Am. J. Sociol. **98**, 1259 (1993).

[4] S. V. Buldyrev, R. Parshani, G. Paul, H. E. Stanley, and S. Havlin, Nature **464**, 1025 (2010).

[5] V. Rosato, L. Issacharoff, F. Tiriticco, S. Meloni, S. D. Porcellinis, and R. Setola, International Journal of Critical Infrastructures **4**, 63 (2008).

[6] A. E. Pereda, Nat. Rev. Neurosci. **15**, 250 (2014).

[7] B. M. Adhikari, A. Prasad, and M. Dhamala, Chaos **21**, 023116 (2011).

[8] X. Song, C. Wang, J. Ma, and J. Tang, Sci. China Technol. Sci. **58**, 1007 (2015).

[9] Y. Xiao, M. Xiong, W. Wang, and H. Wang, Phys. Rev. E **77**, 330 (2008).

[10] B. D. MacArthur, R. J. Sánchez-García, and J. W. Anderson, Discrete Appl. Math. (2008).

[11] R. J. Sánchez-García, E. Cozzo, and Y. Moreno, Phys. Rev. E **89**, 052815 (2014).

[12] M. De Domenico, V. Nicosia, A. Arenas, and V. Latora, Nat. Comm. **6**, 1 (2015).

[13] F. Sorrentino, New J. Phys. **14**, 033121 (2012).

[14] D. Irving and F. Sorrentino, Phys. Rev. E **86**, 056102 (2012).

[15] C. I. del Genio, J. Gómez-Gardeñes, I. Bonamassa, and S. Boccaletti, Science advances **2**, e1601679 (2016).

[16] R. Sevilla-Escoboza, I. Sendiña-Nadal, I. Leyva, R. Gutiérrez, J. M. Buldú, and S. Boccaletti, Chaos **26**, 065304 (2016).

[17] I. Leyva, R. Sevilla-Escoboza, I. Sendiña-Nadal, R. Gutiérrez, J. M. Buldú, and S. Boccaletti, Sci. Rep. **7**, 1 (2017).

[18] L. M. Pecora, F. Sorrentino, A. M. Hagerstrom, T. E. Murphy, and R. Roy, Nat. Comm. **5**, 1 (2014).

[19] I. V. Belykh and M. Hasler, Chaos **21**, 016106 (2011).

[20] M. Wickramasinghe and I. Z. Kiss, PLoS ONE **8**, e80586 (2013).

[21] K. A. Blaha, J. Lehnert, A. Keane, T. Dahms, P. Hövel, E. Schöll, and J. L. Hudson, Physical Review E **88**, 062915 (2013).

[22] N. E. Kouvaris, M. Sebek, A. S. Mikhailov, and I. Z. Kiss, Angewandte Chemie International Edition **55**, 13267 (2016).

[23] F. Sorrentino, L. M. Pecora, A. M. Hagerstrom, T. E. Murphy, and R. Roy, Science Advances **2** (2016).

[24] C. R. S. Williams, F. Sorrentino, T. E. Murphy, and R. Roy, Chaos: An Interdisciplinary Journal of Nonlinear Science **23**, 043117 (2013).

[25] L. Pecora, F. Sorrentino, A. Hagerstrom, T. Murphy, and R. Roy, Nat. Comm. **5**, 4079 (2014).

[26] M. Frasca, L. Gambuzza, A. Buscarino, and L. Fortuna, *Synchronization in Networks of Nonlinear Circuits* (Springer, 2018).

[27] M. Kennedy, IEEE Trans. Circ. Syst. Fund. Theor. Appl. **41**, 771 (1994).

[28] M. Kennedy, IEEE Trans. Circ. Syst. Fund. Theor. Appl. **42**, 376 (1995).

[29] G. M. Maggio, O. De Feo, and M. P. Kennedy, IEEE Trans. Circ. Syst. Fund. Theor. Appl. **46**, 1118 (1999).

[30] A. Uchida, M. Kawano, and S. Yoshimori, Phys. Rev. E **68**, 821 (2003).

[31] L. K. Kana, A. Fomethe, H. B. Fotsin, E. T. Wembe, and A. I. Moukengue, Journal of Nonlinear Dynamics **2017**, 1 (2017).

[32] M. Wickramasinghe and I. Z. Kiss, Physical Review E **88**, 062911 (2013).

[33] M. Kivela, A. Arenas, M. Barthélémy, J. P. Gleeson, Y. Moreno, and M. A. Porter, Journal of Complex Networks **2**, 203 (2014).

[34] S. Boccaletti, G. Bianconi, R. Criado, C. I. Del Genio, J. Gómez-Gardenes, M. Romance, I. Sendina-Nadal, Z. Wang, and M. Zanin, Phys. Rep. **544**, 1 (2014).

[35] M. Tinkham, *Group theory and quantum mechanics* (MacGraw-Hill, New York, NY, 1964).

[36] Y. Xiao, B. D. MacArthur, H. Wang, M. Xiong, and W. Wang, Physical Review E **78**, 046102 (2008).

[37] E. J. Doedel, A. R. Champneys, F. Dercole, T. Fairgrieve, A. Yu, B. Oldeman, R. Paffenroth, B. Sandstede, X. Wang, C. Zhang, *et al.*, (2007).

[38] F. Dercole, SIAM J. Sci. Comput. **30**, 2405 (2008).

[39] A. Dhooge, W. Govaerts, and Y. A. Kuznetsov, ACM Transactions on Mathematical Software (TOMS) **29**, 141 (2003).

[40] Y. A. Kuznetsov, W. Govaerts, E. J. Doedel, and A. Dhooge, SIAM J. Numer. Anal. **43**, 1407 (2005).

[41] V. D. Witte, F. D. Rossa, W. Govaerts, and Y. A. Kuznetsov, SIAM J. Appl. Dyn. Syst. **12**, 722 (2013).

[42] E. Ott, *Chaos in dynamical systems* (Cambridge university press, 2002).

[43] See Supplemental Material ADD URL HERE for a more in depth discussion relating the multilayer network presented in this paper to the state of the field, which includes Refs. [62–67].

[44] E. M. Izhikevich, *Dynamical systems in neuroscience* (MIT press, 2007).

[45] E. M. Izhikevich, IEEE Transactions on Neural Networks **15**, 1063 (2004).

[46] C. Zhou and J. Kurths, Chaos: An Interdisciplinary Journal of Nonlinear Science **13**, 401 (2003).

[47] J. W. Scannell, C. Blakemore, and M. P. Young, Journal of Neuroscience **15**, 1463 (1995).

[48] O. Sporns and R. Kötter, PLoS Biology **2**, e369 (2004).

[49] P. Hagmann, M. Kurant, X. Gigandet, P. Thiran, V. J. Wedeen, R. Meuli, and J.-P. Thiran, PLoS ONE **2**, e597 (2007).

[50] E. T. Bullmore and D. S. Bassett, Annual Review of Clinical Psychology **7**, 113 (2011).

[51] P. Jiruska, M. De Curtis, J. G. Jefferys, C. A. Schevon, S. J. Schiff, and K. Schindler, The Journal of physiology **591**, 787 (2013).

[52] I. V. Belykh and M. Hasler, Chaos: An Interdisciplinary Journal of Nonlinear Science **21**, 016106 (2011).

[53] G. Deffuant, D. Neau, F. Amblard, and G. Weisbuch, Advances in Complex Systems **3**, 87 (2000).

[54] R. Hegselmann, U. Krause, *et al.*, Journal of artificial societies and social simulation **5** (2002).

[55] W. Quattrociocchi, G. Caldarelli, and A. Scala, Scientific reports **4**, 4938 (2014).

[56] F. Della Rossa, S. Fasani, and S. Rinaldi, Mathematical and Computer Modelling **55**, 1562 (2012).

[57] (MDPI, 2018).
[58] H. Cho and E. E. Swartzlander, IEEE Transactions on Nanotechnology **6**, 374 (2007).
[59] J. Cosp, J. Madrenas, E. Alarcon, E. Vidal, and G. Villar, IEEE Trans. on Neural Network **15**, 1315 (2004).
[60] M. Scheffer, S. R. Carpenter, T. M. Lenton, J. Bascompte, W. Brock, V. Dakos, J. van de Koppel, I. A. van de Leemput, S. A. Levin, E. H. van Nes, M. Pascual, and J. Vandermeer, Science **338**, 344 (2012).
[61] M. Alberti, *Cities that think like planets: complexity, resilience, and innovation in hybrid ecosystems* (University of Washington Press, 2016).
[62] M. Berlingerio, M. Coscia, F. Giannotti, A. Monreale, and D. Pedreschi, World Wide Web **16**, 567 (2013).
[63] S. V. Buldyrev, R. Parshani, G. Paul, H. E. Stanley, and S. Havlin, Nature **464**, 1025 (2010).
[64] R. Criado, M. Romance, and M. Vela-Pérez, International Journal of Bifurcation and Chaos **20**, 877 (2010).
[65] J. F. Donges, H. C. Schultz, N. Marwan, Y. Zou, and J. Kurths, The European Physical Journal B **84**, 635 (2011).
[66] J. Gao, S. V. Buldyrev, H. E. Stanley, and S. Havlin, Nature physics **8**, 40 (2012).
[67] S. Gomez, A. Diaz-Guilera, J. Gomez-Gardenes, C. J. Perez-Vicente, Y. Moreno, and A. Arenas, Physical review letters **110**, 028701 (2013).